INSTITUTE OF PHYSICS PUBLISHING JOURNAL OF MICROMECHANICS AND MICROENGINEERING

J. Micromech. Microeng. **17** (2007) 304–313 doi:10.1088/0960-1317/17/2/017

A micromachined high throughput Coulter counter for bioparticle detection and counting

Jiang Zhe[1], Ashish Jagtiani[1], Prashanta Dutta[2], Jun Hu[3] and Joan Carletta[4]

[1] Department of Mechanical Engineering, University of Akron, Akron, OH 44325, USA
[2] Mechanical and Materials Engineering, Washington State University, Pullman, WA 99164, USA
[3] Department of Chemistry, University of Akron, Akron, OH 44325, USA
[4] Department of Electrical and Computer Engineering, University of Akron, Akron, OH 44325, USA

E-mail: jzhe@uakron.edu

Received 7 September 2006, in final form 6 November 2006
Published 11 January 2007
Online at stacks.iop.org/JMM/17/304

Abstract
We describe a micromachined Coulter counter with multiple sensing microchannels for quantitative measurement of polymethacrylate particles and pollen. A unique design with sensing microelectrodes in the center of the microchannels is demonstrated. This design creates isolation resistances among channels, and thus circumvents the crosstalk caused by automatic electrical connection among microchannels. When implemented using microfluidic channels, this design is appropriate for the sensing of microscale particles in deionized water or in dilute electrolyte solution. Our design has multiple channels operating in parallel, but integrated with just one sample reservoir and one power source. The results with a four-channel device show that this device is capable of differentiating and counting micro polymethacrylate particles and Juniper pollen rapidly. Moreover, the device throughput is improved significantly in comparison to a single-channel device. The concept can be extended to a large number of sensing channels in a single chip for significant improvement in throughput.

(Some figures in this article are in colour only in the electronic version)

1. Introduction

Bioactive particles, such as bacteria and pollen, represent an important class of environmental threat to public health. For example, diseases from pathogenic bacteria account for 20 million annual estimated deaths world-wide [1], 76 million illnesses [2] and $9–13 billion in medical costs in the US each year [3]. Additionally, a number of bioparticles such as Anthrax that can be formulated as bioweapons, are potential threats to homeland security [4]. Rapid detection and differentiation of bioparticles is of utmost importance. While authentication services for bioactive particles are currently provided by research laboratories equipped with expensive and bulky set-ups, it is important to develop new analytical devices that are portable, smart, inexpensive and suitable for mass production [1, 5]. These characteristics are necessary for distributed sensor networks and to enable first-responders to pinpoint the source of contamination. Typical requirements for an effective analytical device include the ability to detect single particles in a relatively large sample volume within a short period of time (high throughput), and to distinguish particular particle species in the presence of other particle species (high selectivity).

Coulter counters (also known as resistive pulse sensors) are well-developed devices used to measure the size and concentration of biological cells and colloidal particles suspended in an electrolyte. In Coulter devices, an electrolyte solution containing particles is allowed to pass through a

microchannel separating two compartments or chambers. When a particle flows through the channel, it causes a change in the electrical resistance of the channel. The change in resistance can be measured as current or voltage pulses, which can be correlated to size, shape, mobility, surface charge and concentration of the particles. Because of their simplicity, high sensitivity and reliability, Coulter-type devices have been used for a large number of applications, from the analysis of blood cells [6] to the detection and counting of colloidal beads [7, 8], pollen [9], metal ions [10] and viruses [11]. More recently, a few groups have demonstrated the use of Coulter counter devices with a single nano scale pore/channel for detection of latex particles [8, 12], single molecules [13], DNA [14] and antibody–antigen binding [15]. With standard extraction techniques [16], pathogenic bioparticles including the food poisoning bacteria in solid food can be collected in an electrolyte solution. A Coulter counter can be adapted to detect these bioparticles.

For traditional Coulter counters with a single channel, throughput is proportional to the square of the diameter of the channel. If such a device is adapted to count submicron or nanometer size particles, the diameter of the detector must be made proportionately small, so that the presence of a particle affects the pore's resistance in a significant and measurable way; otherwise, sensitivity of the device is compromised. The result is that single pore devices for counting nanoscale particles can process only a very small volume of sample at a time, and therefore have low throughput. In addition, bioactive particles are generally present at very dilute concentrations. For instance, pathogenic bacteria typically have a concentration of less than 100 Colony-forming units (CFU) per milliliter [17]; as a result, to detect a large volume (>100 ml) of the bioparticle solution without pre-enrichment with a single-channel device would take an impractically long time. While a number of separate Coulter cells can be grouped together to allow passage of a large volume of particle solution [18, 19]. However, it is difficult to integrate a large number of Coulter cells on one chip as each Coulter cell typically has its own power supply, detection electronics and fluidic system in order to avoid electronic coupling (crosstalk) among the Coulter cells.

With the long-term goal to develop a portable high throughput device suitable for micro- and nano-scale bioparticles, we describe a micromachined Coulter counter with multiple sensing microchannels. This device is an improvement on the multichannel devices reported earlier [20, 21] in that this is a micromachined device with microchannels that operate in parallel, using a single sample reservoir and with no need to physically isolate the microchannels. Preliminary results with a four-channel device show that this device is capable of detecting and differentiating micro polymethacrylate particles and pollen rapidly. The device features a unique placement of the sensing electrodes in the middle of the microchannels; with this arrangement, the crosstalk among channels is found to be negligible. The concept can be extended to a large number of sensing channels for significant improvement in throughput without compromising sensitivity and reliability. To our knowledge, such a device has not been reported elsewhere.

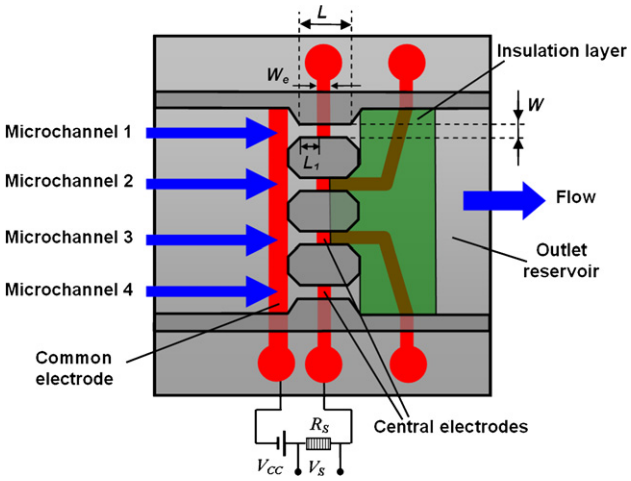

Figure 1. Schematic of the multichannel Coulter counter. The channel height is 50 μm (not shown in the figure).

2. Sensor design and fabrication

2.1. Design and description

The design concept of the device is illustrated in figure 1. The multichannel sensor consists of an inlet reservoir and an outlet reservoir, connected by four microchannels of dimensions 50 μm (H) $\times$100 μm (W) $\times$400 μm (L). The convergent entrance and divergent exit of the microchannel are designed to reduce the energy loss and flow instability. The device has a common electrode placed in the inlet reservoir at the entrance of the microchannels and four central electrodes fabricated at the center of each microchannel. Each central electrode (electrode width $W_e = 100$ μm) is exposed to the electrolyte only at the center of the channel for measurement purposes. The central electrode divides each microchannel into two equivalent half-microchannels of dimensions 50 μm (H) $\times$100 μm (W)$\times$ 150 μm (L_1). The first half channel is used as the sensing channel that counts the particles passing through it, while the second half of the microchannel is used as an isolation resistor to reduce the crosstalk among channels. The measurement setup for one channel is illustrated in figure 1, which consists of a constant dc supply (V_{CC}) connected to the common electrode at one end and to a sampling resistor (R_s) at the other end. The electrolyte containing particles is forced to move from the inlet reservoir to the outlet reservoir through the multiple sensing channels. When a particle passes through a channel, it causes a change in the resistance of the electrolyte-filled first-half microchannel, thereby resulting in a voltage pulse across the sampling resistor for that channel. The voltage pulses across each sampling resistor can be recorded and analyzed separately. In contrast to a single-channel Coulter counter, the sensor can detect particles through its four sensing channels simultaneously; thus, the design enables higher throughput.

2.2. Electrical equivalent of the sensor

Figure 2 shows a simplified electrical model of the multichannel device. The electrical circuit model along with the measurement setup is presented in figure 3. The

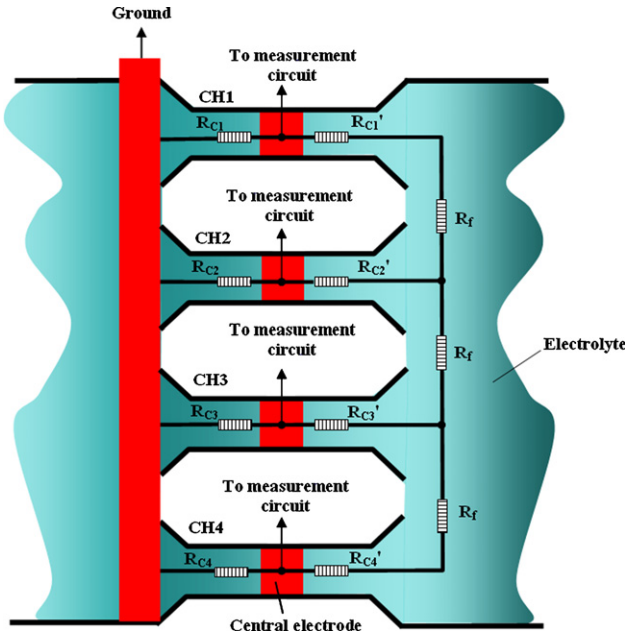

Figure 2. Simplified electrical model of the four-channel device based on the Coulter counting principle. Central electrodes (only active areas are shown) divide each microchannel into two resistors R_{ci} and R'_{ci} ($i = 1, 2, 3, 4$). The resistance R_f formed by the electrolyte solution among two adjacent channels is considered negligible.

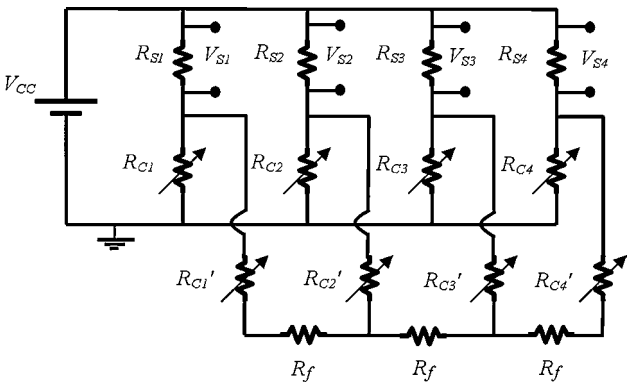

Figure 3. Electrical model of the multichannel Coulter counter. R_{ci}, R'_{ci} and R_{si} represent the first half channel resistance, second half channel resistance (isolation resistance) and the sampling resistor, respectively. R_f is the resistance formed by the electrolyte between two adjacent microchannels.

measurement electrode in the center of a sensing channel divides that channel into two equivalent resistances R_{ci} and R'_{ci} ($i = 1, 2, 3, 4$). The first half of each microchannel (R_{ci}) serves as a sensing channel, while the second half of each microchannel (R'_{ci}) serves as an isolation resistance. When a particle passes through channel i, it affects the equivalent resistance of the first half of the channel, R_{ci}, and then the equivalent resistance of the second half, R'_{ci}. The change is dependent on both the particle size and amount of surface charge [22]. Here R_{si} is the sampling resistor of the microchannel, across which the recorded voltage V_{si} is measured. R_f is the resistance formed by the electrolyte between two adjacent microchannels; this resistance is usually

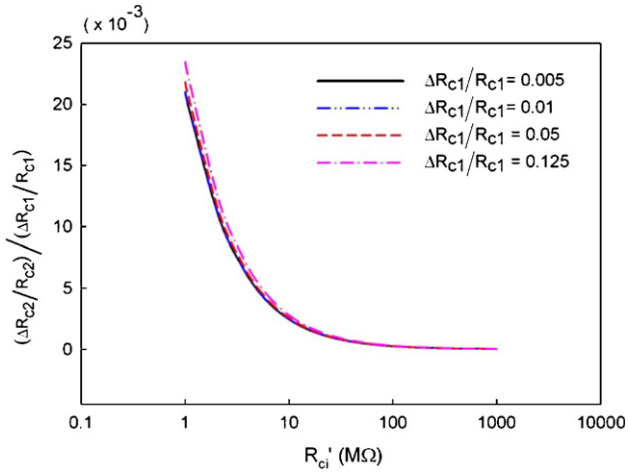

Figure 4. Typical crosstalk analysis between two adjacent microchannels using PSpice®. We assume $R_{ci} = R'_{ci}$ and $R_f = 0$.

small compared to the microchannel resistance and is therefore neglected.

One challenge for using multiple sensing channels is the electronic coupling or crosstalk among channels because the electrolyte electrically connects all channels. When one particle passes through a microchannel, it generates a resistance change in this channel. Because all channels are electrically connected, a resistance change in one channel can possibly cause a current change in other channels, and in turn induce a voltage change across the sampling resistors of other microchannels. This voltage change will be translated into a resistance change signal for other channels where there is no passage of particles, resulting in false detections. The placement of measurement electrodes in the center of microchannels creates an isolation resistor R'_{ci} between each pair of microchannels (see figure 3) and reduces the crosstalk. Figure 4 shows the result of a typical crosstalk analysis of our device using PSpice® assuming $R_{ci} = R'_{ci}$. When the isolation resistance R'_{ci} is 10 MΩ, the relative crosstalk $(\Delta R_{c2}/R_{c2})/(\Delta R_{c1}/R_{c1})$ in other channels is approximately 2.5×10^{-3} and is considered negligible. As the isolation resistance increases, the crosstalk is further reduced. For instance, when $R'_{ci} = 100$ MΩ, the crosstalk $(\Delta R_{c2}/R_{c2})/(\Delta R_{c1}/R_{c1})$ is 2.52×10^{-4}.

The resistance of the microchannel can be estimated by $R = \rho L/A$, where ρ is the resistivity of the electrolyte, L is the length of the microchannel, and A is the cross section of the microchannel. In this work, we use deionized (DI) water, with a resistivity of about 8.33×10^3 Ω m, to carry the microparticles. For the microchannel we used, the estimated resistance of the DI water filled-microchannel (R'_{ci}) is in the order of 100 MΩ; thus, the crosstalk is negligible. Note here that the resistance between microchannels (R_f) is small and negligible compared to the resistances of the microchannels (R_{ci} and R'_{ci} in figure 3). The result is that crosstalk is not particularly dependent on the physical location of the microchannels; crosstalk exists from one channel to all other channels. This means that the analysis is the same for every channel; the crosstalk at the edge channels is no different than those in the middle.

When the channel size is scaled down to nanometer level, according to the scaling law, R'_{ci} will be increased significantly, and thus much less crosstalk should be expected. Therefore while for our microscale device the elimination of crosstalk relies on the use of a carrier fluid with a high resistivity, like deionized water or a very dilute electrolyte, our design should work with negligible crosstalk in nanoscale channels when using a more concentrated electrolyte with its correspondingly lower resistivity. For instance, if the microchannel is scaled down 1000 times to nanometer level ($L = 400$ nm, $W = 100$ nm and $H = 50$ nm), and a more concentrated 0.1 M KCl solution (resistivity $\rho = 0.776\ \Omega$ m) is used, the half channel resistance is 23.3 MΩ; the relative crosstalk will be 1.1×10^{-3}. If an external sampling resistor $R_s = 1$ kΩ is selected, crosstalk will be further reduced to 1.1×10^{-5}. Note that concentrated electrolytes may be necessary for carrying certain bioactive particles. As an example, 0.1 M NaCl is needed to create proper survival conditions (isotonic) for certain cells so that cells do not dehydrate or swell [23].

2.3. Device fabrication

The microchannel and reservoirs were fabricated on polydimethylsiloxane (PDMS) using soft lithography techniques [24], and were bonded to a glass substrate with gold electrodes sputtered on it. Details of PDMS microchannel fabrication techniques were presented elsewhere [25]. Briefly, a positive master of the desired channel thickness (50 μm) was formed using a photolithography technique. First, a photoresist (SU-8 2025, MicroChem, Newton, MA) was spin coated on a glass substrate at 1750 rpm for 35 s and both pre-(at 65 °C for 150 s) and soft-(at 95 °C for 6 min) baked to form a 50 μm thick layer. After near ultraviolet (UV) light (365 nm) exposure at 380 mJ cm^{-2} and post baking (at 95 °C for 5 min), a patterned positive relief is prepared by dissolving the exposed regions for 150 s with the corresponding developer (SU-8 Developer, MicroChem, MA).

Next, the base and curing agent of PDMS (Sylgard 184, Dow Corning, Midland, MI) were mixed at a ratio of 10:1. The prepolymer mixture was degassed in a desiccator with a vacuum pump for 1 h to remove any air bubbles in the mixture. Then, the mixture was poured onto the master to form a 3–5 mm thick PDMS substrate. The PDMS was cured for 3 h at 80 °C on a hot plate. At the end of the curing process, the PDMS layer is peeled off from the glass substrate, and the sample is submerged in acetone for 2 h. Then the PDMS layer is rinsed with DI water and IPA, and blow dried with the compressed air. This PDMS layer was used as the top surface of the sensor.

For fabricating electrodes or sensing elements, 5 nm of titanium tungsten (TiW) was sputtered on a glass substrate followed by 95 nm of gold (Au). Sputtering was carried out in the dc mode for 23 min under a chamber pressure of 7.5×10^{-3} Torr and argon was introduced at a flow rate of 8.16 ml min^{-1}. In the sputtering process, the power levels for TiW and Au were set at 100 W and 75 W, respectively. Electrodes were then created by precise patterning of photoresist (AZ P4620) using contact photolithography [26] and selective etching of gold and TiW thin films from the glass substrate. During the patterning process, a different transparent mask is used to form the particular array of electrodes. Gold not coated by photoresist is etched with trifluoric acetic acid (TFA), rinsed in DI water, and then agitated in 30% hydrogen peroxide for 40 s to remove the titanium tungsten layer. Cleaning with acetone and IPA washes away photoresist, so an array of patterned Au-TiW electrodes is formed on the glass (bottom) layer. The electrode embedded glass slide is then rinsed with DI water, acetone and IPA, and blow dried with compressed air. Next a thin insulation layer (3 μm) of photoresist (AZ P4620) was formed at the selected region using the photolithography technique. The photolithography technique used during the (insulation) patterning process was identical to that described earlier [26], but in this case the spin rate was 3000 rpm.

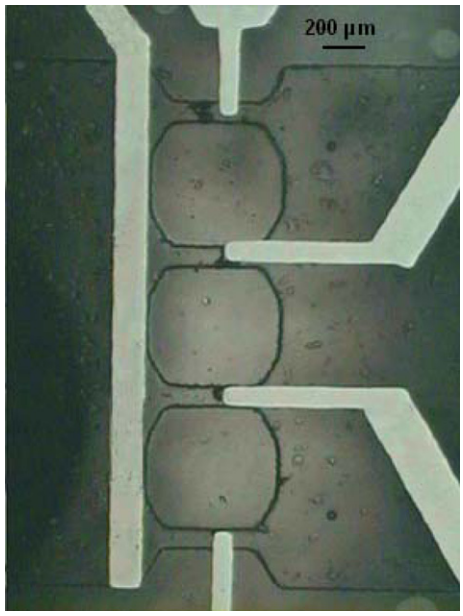

Figure 5. A microscopic picture of the microchannels and the electrodes. The picture is taken from the backside (glass substrate). The insulation layer is not visible.

The PDMS layer with developed channels and electrode-embedded glass slide was then treated with RF oxygen plasma (Plasma Etcher PE 2000, South Bay Technology Inc., San Clemente, CA) for 25 s (50 W, 200 mTorr). This temporarily activated the exposed part of the PDMS and provided very good adhesion. The PDMS replica and glass side were then immediately brought into contact, aligned and bonded together. This hybrid microchip was then rinsed with Nanopure water for several times. Finally, the water is removed from the microchip using compressed nitrogen gas. Figure 5 shows a microscopic picture of the microchannel and the electrodes taken from the backside (glass substrate) of the device. The insulation layer is not visible.

2.4. Particle size calculation

A single measurement channel consists of the half channel resistance R_{ci} in series with the sampling resistor R_s and the supply voltage (see figure 1). When a particle passes through the microchannel it causes a change in the resistance (R_{ci}), and a corresponding change in the voltage across the sampling

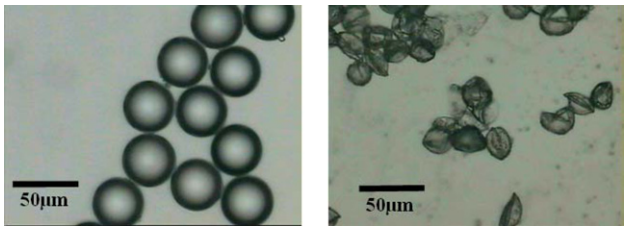

(*a*) (*b*)

Figure 6. Optical microscope pictures of (*a*) 40 μm PMA particles and (*b*) Juniper Scopulorum tree pollen.

resistor. The relative change in resistance of the microchannel in terms of the measured voltage is given by

$$\frac{\delta R_c}{R_c} = \frac{(V_s - V_s')V_{CC}}{(V_{CC} - V_s)V_s'} \tag{1}$$

where V_s' is the measured voltage when a particle is present in the microchannel and V_s is the measured voltage in the absence of a particle in the microchannel.

For a micro-channel with length L and diameter D, the change in resistance as a particle passes through it is given by [7]

$$\frac{\delta R_c}{R_c} = \frac{d^3}{LD^2}\left[\frac{D^2}{2L^2} + \frac{1}{\sqrt{1+\left(\frac{D}{L}\right)^2}}\right] \cdot F\left(\frac{d^3}{D^3}\right) \tag{2}$$

where d is the diameter of the particle and $F(d^3/D^3)$ is a correction factor. For the rectangular microchannel, we used the characteristic diameter $D = \sqrt{4A/\pi}$ in equation (2), where A is the cross-sectional area of the microchannel. For the 50 μm $\times$ 100 μm microchannel used in the sensor, the characteristic diameter D is calculated as 80 μm. The correction factor F is 1 for $(d/D)^3 < 0.1$ [7]. For 40 μm polymethacrylate particle, $(d/D)^3 = 0.125$ and the correction factor is taken as 1.174 [7]. Thus, the particle diameter can be calculated from the relative change in resistance as

$$d = \left(\frac{\frac{\delta R_c}{R_c} LD^2 \Big/ F\left(\frac{d^3}{D^3}\right)}{\frac{D^2}{2L^2} + \frac{1}{\sqrt{1+\left(\frac{D}{L}\right)^2}}}\right)^{\frac{1}{3}}. \tag{3}$$

3. Materials and experimental setup

3.1. Tested particle samples

Two different particle types were investigated as models: polymethacrylate (PMA) particles with well-characterized diameters of 40 μm (40.15 μm $\pm$ 0.76 μm) (Sigma Aldrich Inc.) and Rocky mountain Juniper (Juniper Scopulorum) tree pollen (Sigma Aldrich Inc.). For PMA particles, the certificate of analysis from Sigma Aldrich indicates that the calibrated particle diameter is 40.15 μm and the standard deviation is 0.76 μm. These particles were chosen because (a) they are commercially available, and (b) PMA particles have well-characterized properties. The diameters of pollen particles were determined using high resolution optical microscopy. The Juniper tree pollen is irregular in shape and the diameter ranges from 17 μm to 23 μm. Figures 6(*a*) and (*b*) show microscope pictures of 40 μm PMA particles and Juniper tree pollen, respectively.

3.2. Measurement procedure

The particle solution is forced to flow through the microchannels by creating a pressure difference with a syringe. An input voltage of $V_{CC} = 6$ V was applied across the microchannels. Due to the polarization effect of the gold electrodes [22], such a high source voltage is necessary to ensure that there is sufficient current/electric field within the electrolyte to record a noticeable voltage change across the sampling resistors. Voltage measurements were made across a sampling resistor $R_s = 100$ kΩ. The voltage trace was recorded for four channels using a National Instruments NI-6220 data acquisition board, with a sampling frequency of 50 kHz.

It should be noted here that the application of a 6 V dc voltage might cause electrolysis of water and generate gas bubbles. The gas bubbles could result in false peaks when they pass through the microchannel. During our experiments, we did not observe obvious gas bubbles on the surfaces of the electrodes and in the solution. This is because of the low current and the gas solubility in the water. Using Stoichiometric equations based on Faraday's law of electrolysis [27] we estimated that the volume rate for oxygen gas and hydrogen gas generated at the electrodes due to electrolysis is 63.8×10^{-9} ml s^{-1} and 127.59×10^{-9} ml s^{-1}. The volume flow rate of the electrolyte solution in our experiment is approximately 5×10^{-6} l s^{-1}, thus the volume of the generated oxygen and hydrogen per liter of electrolyte solution is 12.8×10^{-3} ml l^{-1} and 25.52×10^{-3} ml l^{-1}, respectively. They are much smaller than the gas solubility in water (5.57 ml l^{-1} for oxygen [28] and 174 ml l^{-1} for hydrogen [29]).

4. Results and discussions

4.1. Counting of 40 μm PMA particles

The sample solution for the 40 μm PMA particle was prepared by taking 0.2 ml of the original solution (10% solid) and diluting in 5 ml water. The estimated original particle concentration was calculated as 9.96×10^4 ml^{-1}. The particle solution is loaded into the inlet reservoir of the device and is forced to flow to the outlet using a syringe, which is controlled manually. The voltage across the sampling resistor R_s is continuously monitored across the four sampling resistors. Figure 7 shows the relative resistance change of the four channels as a function of time, converted from voltage traces measured across the four sampling resistors using equation (1). In figure 7, pulses appear in random sequence, with no correlation among the pulses in different channels; this implies that the four sensing channels were able to simultaneously generate voltage pulses and count particles without crosstalk among channels. An unbiased cross correlation analysis was performed between the signals from two sensing channels at a time. The typical result is plotted in figure 8. It is obvious that the cross correlation coefficients $|r|$ are less than 0.1, indicating that there is negligible correlation among the pulses of different channels.

Because each resistive pulse represents a particle passing through one microchannel, the concentration of the particles in the four channels was calculated from the number of

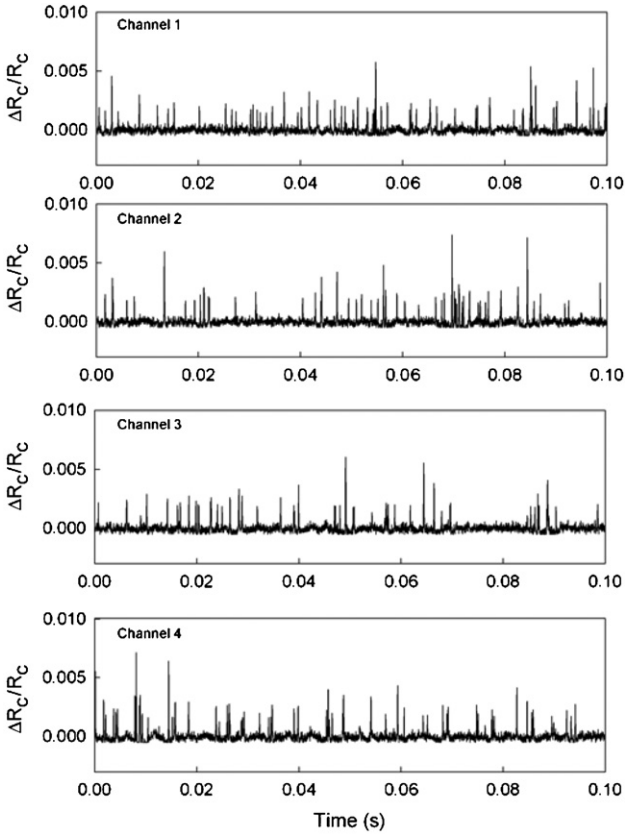

Figure 7. Relative resistance change across four microchannels for 40 μm PMA particles.

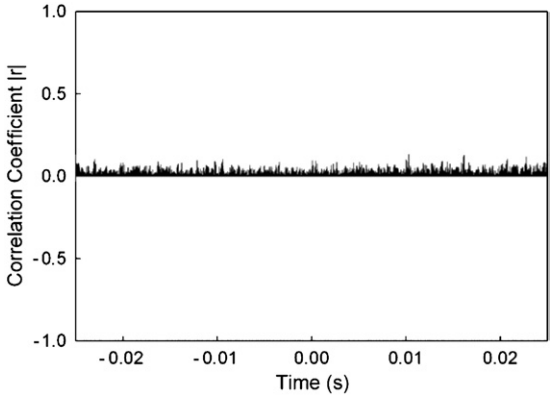

Figure 8. Cross correlation results of two channel data for 40 μm PMA particles indicating $|r| < 0.1$.

pulses during a period of 1 s. As a result, the measured concentrations are 9.58×10^4 ml^{-1}, 8.34×10^4 ml^{-1}, 7.06×10^4 ml^{-1} and 10.17×10^4 ml^{-1} for channels 1 to 4, respectively. A comparison of the measured concentration and sizes with the expected original concentration and sizes are shown in figure 9. Because of the manual flow rate control, there exist uncertainties in the estimation of the flow rate and thus the measured concentration. The error bars of the concentration columns in figure 9 represent the uncertainties in the measured concentrations. It can be seen from figure 9 that the measured concentrations are comparable to the expected original concentration. The difference between the measured

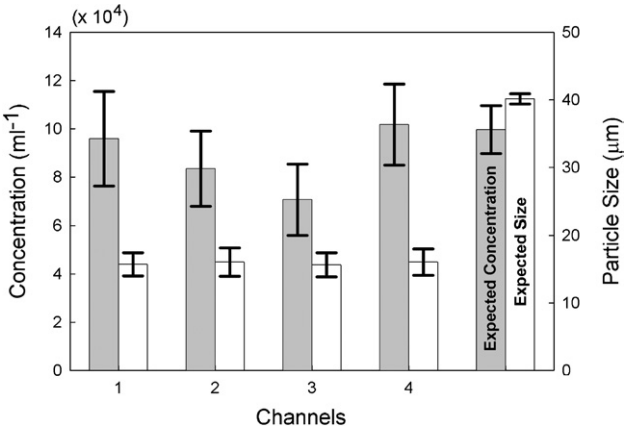

Figure 9. Comparison of measured concentration and size for 40 μm PMA particles with the expected original concentration and size.

concentrations and the expected concentration is due to the particle deposition onto the substrate during the experiments, dilution errors and non-uniform mixing of the solution. While we sonicated the particle solutions in an ultrasonic bath before the experiment to reduce the particle aggregation, it is still possible that two particles might aggregate and cause a larger pulse. This might account for the occasional large peaks in figure 7 and the slightly lower particle concentration.

The relative change in resistance was used to calculate the particle diameters using equation (3). The resulting measured sizes of the PMA particles are 15.7 $\pm$ 1.7 μm for channel 1, 16.03 $\pm$ 2.1 μm for channel 2, 15.62 $\pm$ 1.8 μm for channel 3, and 16.04 $\pm$ 1.97 μm for channel 4. The error bars shown in the particle size columns in figure 9 represent the standard deviation in particle size. The large difference between the measured and the expected particle diameter (40.15 μm $\pm$ 0.76 μm) is mainly because of the polarization effect that takes place on the gold electrodes. In the electrolyte solution and DI water, electrode polarization causes the dc voltage applied on electrodes to be dropped across the double layers of the two electrodes. Thus, the voltage drop across the bulk solution is less than the actual applied voltage [30], resulting in underestimated particle dimensions when equation (3) is used. The electrode polarization can be reduced by using Ag/AgCl electrodes with large surface areas [30]. In our previous study [9, 20, 21], Ag/AgCl electrodes (1 mm in diameter and 4 cm in length) were used in a meso-size Coulter counter to analyze the PMA particles. The measured size of the PMA particles was close to the expected size. Because of the limited life time for microscale Ag/AgCl electrodes [31], we used gold electrodes in this study to demonstrate the concept of a multichannel Coulter counter for rapid counting of microparticles.

4.2. Counting of Juniper pollen

The Juniper pollen particle solution was prepared by diluting 10 mg of Juniper tree pollen in 10 ml of water. Taking an estimated density of 1.1 gm cm^{-3} and an average diameter of 20 μm for the Juniper pollen, the concentration of the prepared pollen sample solution was estimated as 2.39×10^5 ml^{-1}. The prepared particle solution is added

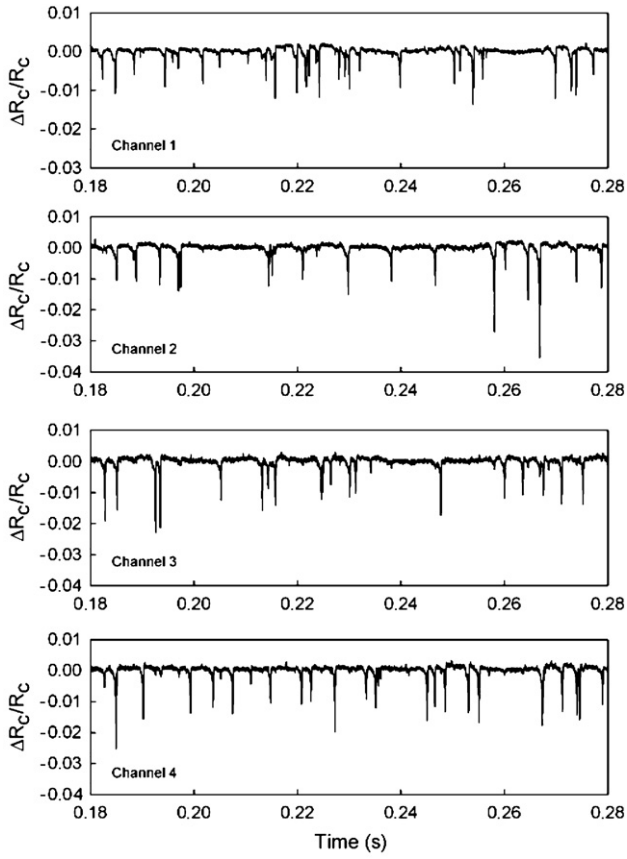

Figure 10. Typical relative resistance change for the Juniper pollen monitored across the four channels.

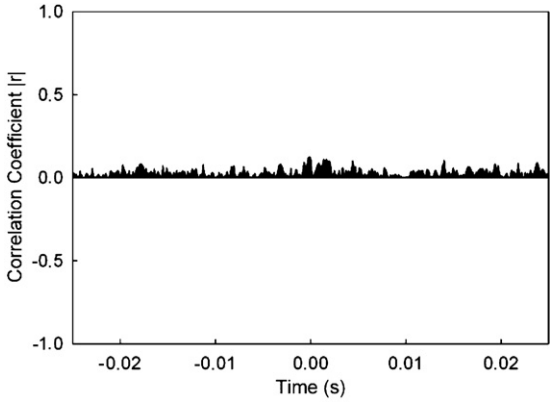

Figure 11. Typical cross correlation results obtained from measurement signals of adjacent channels for tree pollen data. The cross correlation coefficient $|r| < 0.1$ indicates negligible crosstalk.

to the inlet reservoir using a syringe. Pressure-driven flow created by the manually controlled syringe forces the particle solution to move toward the outlet reservoirs through the four sensing microchannels. The voltage across the sampling resistor R_s is continuously monitored across the four sampling resistors. Figure 10 shows the relative resistance change of the four channels as a function of time, converted from voltage traces measured across the four sampling resistors using equation (1). Each resistive pulse represents one pollen particle passing through a microchannel. The resistive traces

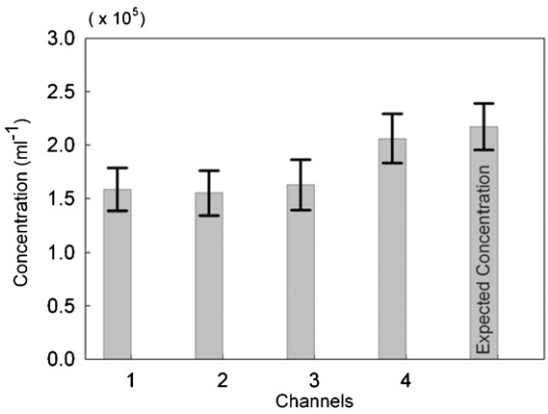

Figure 12. Measured concentration of Juniper Tree pollen compared to the expected concentration.

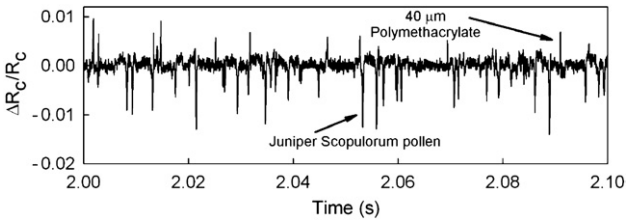

Figure 13. Typical relative resistances for a mixture of Juniper tree pollen and 40 μm PMA particles in one channel of the device.

show pulses appearing in random sequence. A similar cross correlation analysis as we conducted in PMA particle counting (section 4.1) was performed between the signals from two sensing channels at a time. The results are shown in figure 11. We found that the cross correlation coefficients $|r|$ are less than 0.1, indicating that there is negligible correlation among the pulses of different channels. This implies that the four sensing channels were able to simultaneously detect and count particles with negligible crosstalk among channels.

It is obvious from figure 10 that the resistive pulses caused by Juniper pollen were all downward, that is, when a pollen particle passes through the microchannel, the microchannel resistance decreases. This phenomenon had been reported in our prior study [9, 20, 21], which pointed out that a particle affects the micro-channel resistance in two competing ways. First, it displaces the electrolyte solution in the microchannel, thereby reducing the number of free ions inside the micro-channel, which leads to an increase in resistance; second, if it has surface charge, it brings additional charges into the micro-channel, which leads to a decrease in resistance. From the experimental results, it appears that the pollen particles have high surface charge, while the PMA particles are only slightly charged or non-charged. For PMA particles, the first factor is dominant. The resistive pulses generated by PMA particles are directly related to their size (equation (3)). However, for pollen particles, because the surface charge is high and the concentration of ions in the DI water is low, the second factor is dominant, and the overall effect of a pollen particle passing through a micro-channel is a downward resistive pulse. A similar phenomenon was reported by Chang *et al* [22], where a negatively charged DNA molecule generated an upward current pulse (a downward resistive pulse) when it

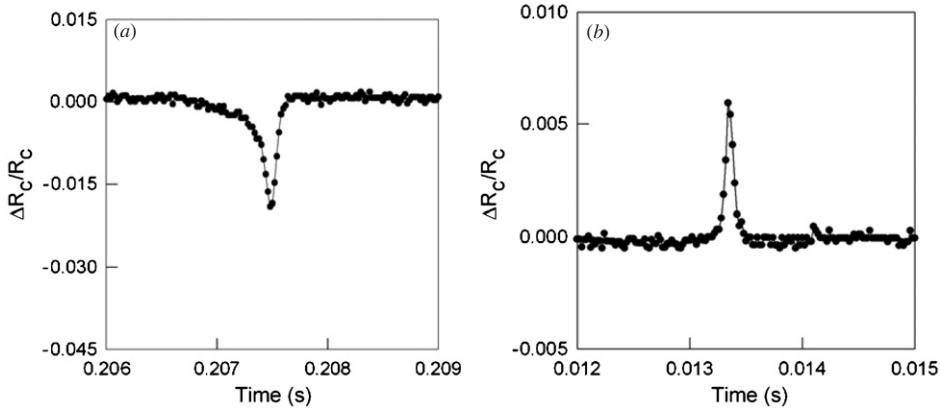

Figure 14. Magnified relative resistive pulses generated by (*a*) Juniper Scopulorum tree pollen, (*b*) 40 μm PMA particles.

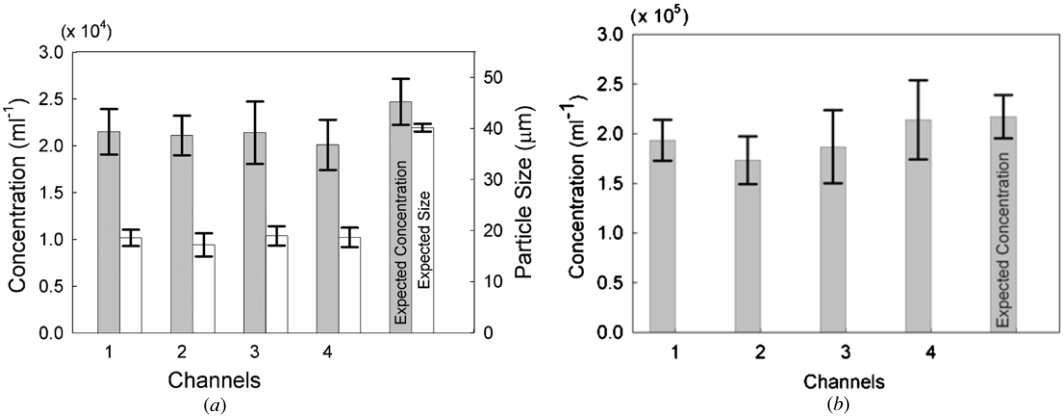

Figure 15. (*a*) Summary of the measured diameter and concentration of 40 μm PMA particles in the mixture. Expected size defined by vendor's CoA specification. The expected concentrations are plotted for comparison; (*b*) measured concentration of Juniper tree pollen compared to estimated original concentration.

passed through a nanopore. This phenomenon can be used to differentiate particles with different surface charges. In our experiment, the pulses of the Juniper pollen vary in height; the variation might be attributed to the surface charge variation and the irregular shape of Juniper pollen.

The concentration of the Juniper pollen in the four channels was calculated from counting the number of downward peaks during the period of 1 s; the concentrations were found to be 1.58×10^5 ml^{-1}, 1.55×10^5 ml^{-1}, 1.63×10^5 ml^{-1} and 2.06×10^5 ml^{-1} for channels 1, 2, 3 and 4, respectively. These results are shown in figure 12. Similar to the testing with PMA particles, the measured pollen particle concentration is lower than the estimated pollen concentration. This is because of particle deposition onto the substrate during the experiments, dilution errors and non-uniform mixing of the solution.

4.3. Counting of 40 μm PMA particles and Juniper pollen mixture

In this experiment, 0.1 ml of 40 μm PMA particles (40.15 ± 0.76 μm diameter, 10% solid) and 10 mg Juniper pollen were mixed in 10 ml DI water and were tested in the multichannel device. The resulting concentration of 40 μm PMA particles and pollen particles is 2.49×10^4 ml^{-1} and 2.39×10^5 ml^{-1} respectively, assuming the density of Juniper pollen is 1.1 g ml^{-1}. The mixed particle solution is added to the inlet reservoir using a syringe. Pressure difference created by the syringe forces the particle solution to move toward the outlet reservoir through the multiple sensing microchannels. Voltage traces across the sampling resistors were recorded. A typical resistive pulse trace in one channel (channel 3) converted from the voltage trace signal is shown in figure 13. It can be observed that PMA and pollen particles generated the similar resistive pulses as those generated in sections 4.1 and 4.2 when the two particles were tested alone. Magnified views of resistive pulses generated by Juniper pollen and 40 μm PMA particles are shown in figure 14. It is obvious that pollen generated downward resistive pulses, while PMA particles generated upward resistive pulses. Thus we are able to differentiate and count the two particle species in the mixture. The concentration of the 40 μm PMA particles in the four channels was calculated by counting the number of upward peaks during the period of 1 s; the concentrations were found to be 2.15×10^4 ml^{-1}, 2.11×10^4 ml^{-1}, 2.14×10^4 ml^{-1}, and 2.01×10^4 ml^{-1} for channels 1, 2, 3 and 4, respectively. These results are shown in figure 15(*a*). The measured particle concentration in each channel is slightly

lower than the estimated particle concentration, which was 2.49×10^4 ml^{-1}.

The particle diameters were calculated from resistive pulse data shown in figure 13 using equations (2) and (3). Using the nominal sensing microchannel (first-half of microchannel) dimension of 50 μm (H) $\times$ 100 μm (W) $\times$ 150 μm (L_1), the analysis shows the estimated particle diameter is 18.5 $\pm$ 1.6 μm, 17.2 $\pm$ 2.3 μm, 18.96 $\pm$ 1.8 μm, and 18.66 $\pm$ 1.9 μm for channels 1, 2, 3 and 4, respectively (see figure 15(*a*)). The error bars shown in figure 15(*a*) represent the standard deviation in particle diameter. As discussed in section 4.1, the large difference between the expected and the measured particle diameter (40.15 μm $\pm$ 0.76 μm) is mainly because of the polarization effect that takes place on the gold electrodes. The polarization effect causes the dc voltage applied on the electrodes be dropped across the double layers of the two electrodes, resulting in underestimated particle dimensions when equation (3) is used.

Similarly, the concentrations of the pollen particles in the four channels were calculated from counting the number of downward peaks during the period of 1 s; the concentrations were found to be 1.93×10^5 ml^{-1}, 1.73×10^5 ml^{-1}, 1.86×10^5 ml^{-1} and 2.14×10^5 ml^{-1} for channels 1, 2, 3 and 4, respectively. Because of the same reason as PMA particles, the measured concentration is lower than the estimated concentrations. The results are shown in figure 15(*b*).

5. Conclusions

A micromachined high throughput Coulter counter for differentiation and counting of Juniper tree pollen and polymethacrylate microparticles has been demonstrated. A unique feature of the design is the placement of microelectrodes in the center of the microchannel. With this feature, isolation resistances between each pair of channels are created, and thus crosstalk is reduced. We found this design effective in removing crosstalk among channels, thus enabling the use of multiple channels in a single device with a single set of detection electronics. The design can be implemented with microscale channels for the analysis of micron scale particles present in electrolyte solution in very low concentration, or with nano-scale channels for the assay of nano-particles at higher concentrations. The microchip sensor demonstrated here utilized four microchannels, all operating simultaneously, to count microparticles such as Juniper tree pollen and polymethacrylate particles. The counting efficiency is improved approximately 300% over that of a single-channel Coulter counter. This microfluidic-based sensor is also capable of differentiating pollen and polymethacrylate particles. The concept, demonstrated here on a four-microchannel sensor, can be extended to a large number of sensing channels in a single chip to further improve the counting efficiency.

Acknowledgments

This work is partially supported by a Faculty Research Grant from The University of Akron and a grant from the Ohio Space Grant Consortium.

References

[1] Ivnitski D, Abdel-Hamid I, Atanasov P, Wilkins E and Stricker S 2000 Review: application of electrochemical biosensors for detection of food pathogenic bacteria *Electroanalysis* **12** 317–25

[2] Mead P S, Slutsker L, Dietz V, Mccraig L F, Bresce J S, Shapiro C, Griffin P M and Tauxe R 1999 Food-related illness and death in the United States *Emerg. Infect. Dis.* **5** 607–25

[3] Buzby J C D, Roberts T, Lin C J and MacDonald J M 1996 Bacterial food borne disease: medical costs and productivity losses *Agricultural Economics Reports* no. 741 (Washington DC: USDA Economic Research Services) p 100

[4] Matsumoto G 2003 Anthrax powder: state of the art? *Science* **302** 1492–7

[5] Guthrie E and Folkerts W 2005 Application notes: detection bioterrorism *Am. Biotechnol. Lab.* **23** 8–9

[6] Zimmermann U, Pilwat G and Riemann F 1974 Dielectric breakdown of cell membranes *Biophys. J.* **14** 881–99

[7] DeBlois R W and Bean C P 1970 Counting and sizing of submicron particles by the resistive pulse technique *Rev. Sci. Instrum.* **41** 909–15

[8] Saleh O A and Sohn L L 2001 Quantitative sensing of nanoscale colloids using a microchip Coulter counter *Rev. Sci. Instrum.* **72** 4449–51

[9] Zheng Z, Zhe J, Chandra S and Hu J 2005 An electronic pollen detection method using Coulter counting principle *Atmos. Environ.* **39** 5446–53

[10] Braha O, Gu L Q, Zhou L, Lu X, Cheley S and Bayley H 2000 Simultaneous stochastic sensing of divalent metal ions *Nature Biotechnol.* **18** 1005–7

[11] DeBlois R W and Wesley R K 1977 Sizes and concentrations of several type C oncornaviruses and bacteriophage T2 by the resistive-pulse technique *J. Virol.* **23** 227–33

[12] Ito T, Sun L, Henriquez R R and Crooks R M 2004 A carbon nanotube-based Coulter nanoparticle counter *Accounts Chem. Res.* **37** 937–45

[13] Bayley H and Martin C R 2000 Resistive-pulse sensing—from microbes to molecules *Chem. Rev.* **100** 2575–94

[14] Kasianiwicz J J, Brandin E, Branton D and Dreamer D W 1996 Characterization of individual polynucleotide molecules using a membrane channel *Proc. Natl Acad. Sci.* **93** 13770–73

[15] Saleh O A and Sohn L L 2003 Direct detection of antibody-antigen binding using an on-chip artificial pore *Proc. Natl Acad. Sci.* **100** 820–4

[16] Zhao X, Hillard L R, Mechery S J, Wang Y, Bagwe R P, Jin S and Tan W 2004 A rapid bioassay for single bacterial cell quantitation using bioconjugated nanoparticles *Proc. Natl Acad. Sci.* **101** 15027–32

[17] Wu J 2006 Biased AC Electro-osmosis for on-chip bioparticles processing *IEEE Trans. Nanotechnol.* **5** 84–9

[18] Coulter W H and Hogg W R 1969 Particle analyzing apparatus and method utilizing multiple apertures *US Patent* 3,444,463

[19] Carbonaro A and Sohn L L 2005 A resistive-pulse sensor chip for multianalyte immunoassays *Lab Chip* **5** 1155–60

[20] Jagtiani A V, Zhe J, Hu J and Carletta J 2006 Detection and counting of micro-scale particles and pollen using a multi-aperture Coulter counter *Meas. Sci. Technol.* **17** 1706–14

[21] Jagtiani A V, Sawant R and Zhe J 2006 A label-free high throughput resistive-pulse sensor for simultaneous differentiation and measurement of multiple particle-laden analytes *J. Micromech. Microeng.* **16** 1530–9

[22] Chang H, Kosari F, Andreadakis G, Alam M A, Vasmatzis G and Bashir R 2004 DNA-mediated fluctuations in ionic current through silicon oxide nanopore channels *Nano Lett.* **4** 1551–6

[23] Matthews G G 2003 *Cellular Physiology of Nerve and Muscle* (Oxford: Blackwell)
[24] Duffy D C, McDonald J C, Schueller J A and Whitesides G M 1998 Rapid prototyping of microfluidic systems in poly(dimethylsiloxane) *Anal. Chem.* **70** 4974–84
[25] Mamun N H and Dutta P 2006 Patterning of platinum microelectrodes in polymeric microfluidic chips *J. Microlithogr. Microfabr. Microsyst.* **5** 039701–63
[26] Salgado J C, Horiuchi K and Dutta P 2006 A conductivity based interface tracking method for microfluidic application *J. Micromech. Microeng.* **16** 920–8
[27] Ramsden E 2001 *Chemistry* 2nd edn (London, UK: Nelson Thornes) pp 294–6
[28] Carpenter J H 1966 New measurements of oxygen solubility in pure and natural water *Limnol. Oceanogr.* **11** 264–77
[29] Weisenburg D A and Guinasso N L Jr 1979 Equilibrium solubilities of methane carbon monoxide, and hydrogen in water and sea water *J. Chem. Eng. Data* **24** 356–60
[30] Saleh O A 2003 A novel resistive pulse sensor for biological measurement *PhD Dissertation* Princeton University, Department of Physics
[31] Guzmán K A D, Karnik R N, Newman J S and Majumdar A 2006 Spatially controlled microfluidics using low-voltage electrokinetics *J. Microelectromech. Syst.* **15** 237–45